# Swirl Combustor Flow Visualization Studies in a Water Tunnel

J. A. Schetz,* P. W. Hewitt,† and R. Thomas†
*Virginia Polytechnic Institute and State University, Blacksburg, Virginia*

**The flowfield in a swirl combustor with a confinement ratio of 1.0, secondary downstream injection, aspiration holes, and a large central hub was simulated. Data was collected from visualization with neutral density plastic beads in water and velocity and turbulence measurements in cold air. The baseline case produced negligible recirculation. Increasing the confinement ratio to 2.1 by insert rings strengthened the central zone to a state of incipient recirculation. Use of a convergent/divergent ring after the swirler had further beneficial effects. The bypass flow reduced the radial size and intensified the incipient recirculation. Extended hubs, although having little effect in the burner, produced a rotating helix in the afterburner.**

## Nomenclature

$A_b$ = area of burner can
$A_s$ = area of swirler section
$C(\bar{t})$ = concentration
$D$ = diameter
$D_b$ = diameter of burner can
$D_s$ = diameter of swirler section
$G_x$ = axial flux of axial momentum
$G_\phi$ = axial flux of swirl momentum
$L_c$ = combustor length from baseline central hub face to exit plane
$P$ = pressure
$Re$ = Reynolds number of model
$Re_0$ = operational Reynolds number of ramjet hardware
$R_b$ = radius of burner can
$R_s$ = radius of swirler section
$r$ = radial coordinate
$S$ = swirl number
$t$ = time
$\bar{t}$ = dimensionless mean residence time
$T$ = temperature
$T_s$ = steady-state temperature
$T_0$ = steady-state temperature with tracer flow
$u'$ = fluctuations in total velocity
$U$ = total velocity
$U_0$ = bulk velocity
$U_x$ = axial velocity
$U_\theta$ = tangential velocity
$\sqrt{u'^2}/U$ = turbulence level
$X$ = axial distance

## Introduction

THE design and development of an efficient combustion chamber involves interrelated flow and chemical processes. While there has been considerable progress in developing computer codes to predict these processes, most, if not all, of the development work is now done by testing. When and if the codes replace any significant portion of that testing, a prudent designer will still insist on testing to verify the computer predictions for the final configuration.

Even subscale testing of combustion chambers is a complex and expensive business, so that it is not an efficient means of investigating a large number of design configurations. Fortunately, in some cases physical fluid flow and chemical effects can be tested separately. In particular, it has proven useful to study the flameholder under cold-flow conditions, and flow visualization in a transparent model with water as the fluid medium is the most common procedure. This paper presents the results of applying this method, and two extensions, to ramjet combustion chambers with swirl.

Swirling flow flameholders are distinguished from conventional flameholders by a toroidal recirculation flow near the entrance of the burner, as shown in Fig. 1. With flameholding accomplished aerodynamically, pressure drops can be reduced. In addition, the high turbulence throughout the recirculation zone can increase combustion intensity shortening combustion chambers. These advantages are critical to the performance of a ramjet, thus making use of swirl flameholding particularly attractive.[1]

Swirling flows are generated by adding a tangential velocity component to an axial flow. The resulting centrifugal forces must be balanced by radial pressure gradients, resulting in a low static pressure near the centerline. Axial expansion of the swirling flow into an unconfined region will result in overall positive axial pressure gradients. These gradients are derived from a pressure rise due to both expansion and increased tangential velocity decay from mixing.[2] Thus the fluid near the axis will see a strong positive pressure gradient downstream from the low static pressure region just after the swirl generator. If this axial pressure gradient is sufficient to overcome axial momentum, then vortex breakdown will occur consisting of a free stagnation point and flow reversal called a central recirculation zone (CRZ) (see Fig. 1). A more complex flow is formed if the flow issues into a confined region of greater diameter. The high entrainment of a swirling turbulent jet cannot be satisfied by the limited fluid in the corner, and the entrainment at the exit of the smaller region must be satisfied by drawing fluid upstream. The effect is to cause attachment of the swirling jet to the wall and thus create a peripheral recirculation zone (PRZ). The intensity of the swirl is usually characterized by a swirl number:

$$S \equiv G_\phi / (G_x R_s) \tag{1}$$

where

$$G_\phi = \int_0^{R_s} (U_\theta r) \rho U_x 2\pi r dr \tag{2}$$

$$G_x = \int_0^{R_s} (U_x) \rho U_x 2\pi r dr + \int_0^{R_s} P \cdot 2\pi r dr \tag{3}$$

and $R_s$ is the radius of the exit to the expansion region, although some have found that $R_b$ may provide better

Presented as Paper 82-1238 at the AIAA/SAE/ASME 18th Joint Propulsion Conference, Cleveland, Ohio, June 21-23, 1982; submitted July 12, 1982; revision received Feb. 15, 1983. 

*Professor and Department Head, Aerospace and Ocean Engineering. Associate Fellow AIAA.
†Graduate Assistant, Aerospace and Ocean Engineering Department. Student Member AIAA.

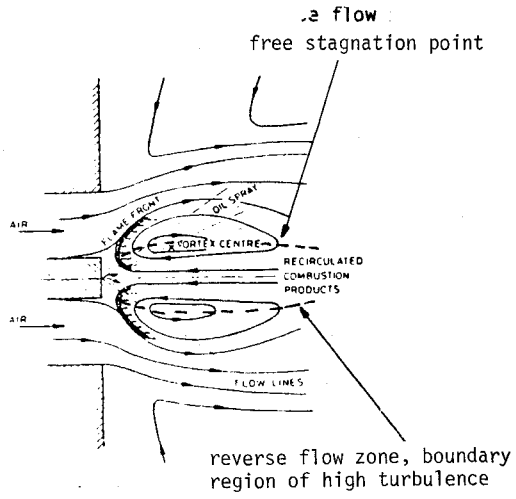


**Fig. 1 Stabilization of flame by central recirculation zone in a swirling annular jet.[7,9]**

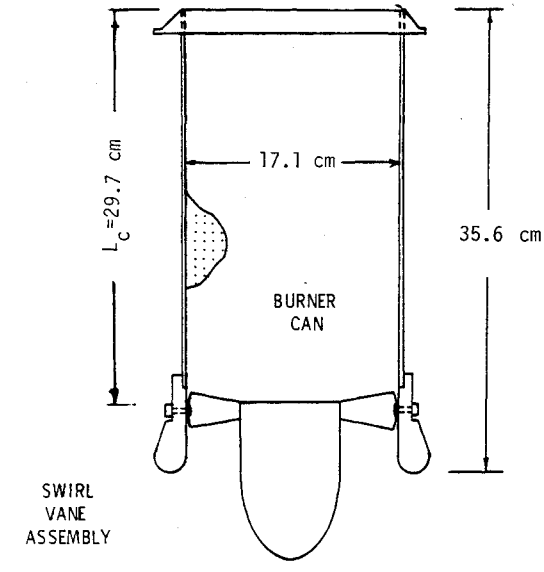


**Fig. 3 Diagram of the 15.2-cm (6-in. nominal) burner can model.**

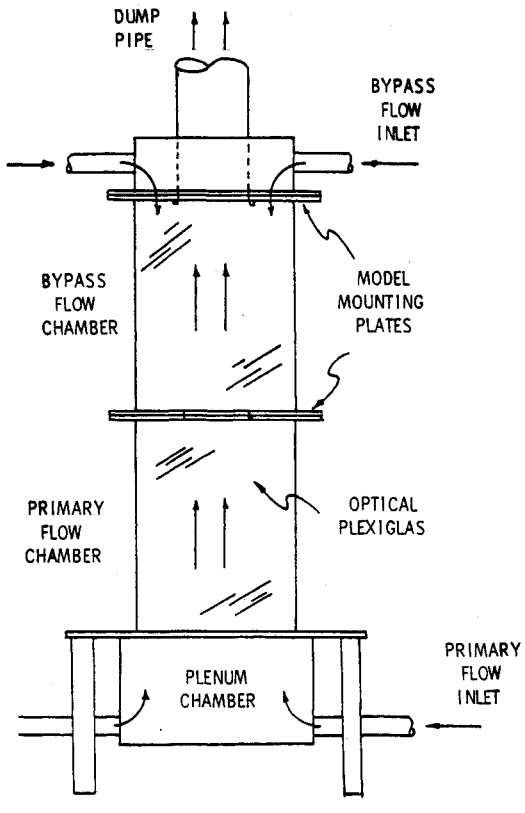


**Fig. 2 Schematic of water flow facility.**

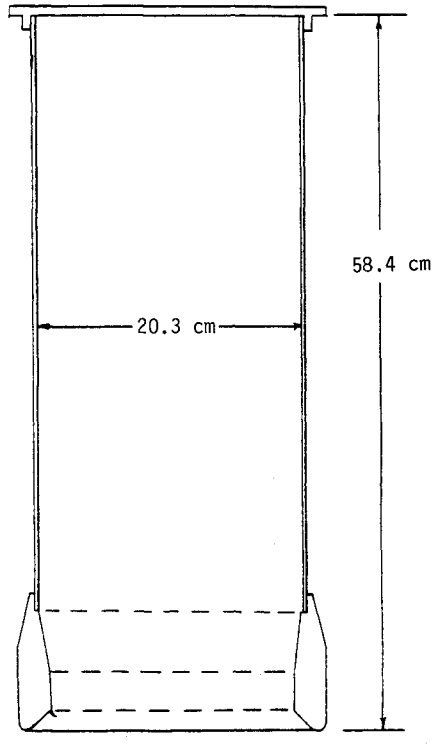


**Fig. 4 Diagram of afterburner model.**

correlations under moderate to high confinement.[3] For high swirl ($S>1.6$), the PRZ may never form, since the flow sticks immediately to the wall. Obviously, the confinement ratio can have large effects on the aerodynamics, flame size and shape, heat transfer, and blowoff limits, particularly when $A_b/A_s<4$ and $S>0.5$ (Ref. 2). This will occur in missiles, the major current application of ramjets.

There are two other features of ramjets that further complicate swirl burners for that application as opposed to industrial furnaces, for example. First, ramjets often burn near stoichiometric, placing severe requirements on the burner lining. This usually necessitates centerbody fuel injection and aspiration cooling holes in the burner can. Second, increased fuel efficiency is always desirable, since performance can be dramatically improved. Downstream injection of cold bypass flow much like that of a turbofan engine has been suggested as a means to provide this economy. A swirl combustor designed to incorporate these features will be an advanced configuration, since these features, combined, are a significant departure from previously researched swirl combustors.

## Methods of Investigation

### Water Flow Visualization

Transparent models of combustors and simulation of hot reacting flow with water are widely used in the development of combustors.[3-5] Combustion produces only small changes in some basic flowfield features. Recirculation boundaries and mass flow rates, for example, are only slightly reduced with combustion.[6]

Small polypropylene isotactic beads can be injected in the flow. With a density within 2% of that of water, the beads follow the streamlines of the flow, providing excellent visualization.

In order to simulate the real flow as accurately as possible, it would be desirable to match the Reynolds number. A matching of the Reynolds number is not feasible even when the model is full scale. The mismatch arises because of a limitation of about 0.3 m/s on water speed to obtain good visualization. It is necessary, however, to have the Reynolds number well above that to guarantee fully turbulent flow. It has been found that a swirling flow with $Re_D \geq 1.8 \times 10^4$ and $S > 0.6$ will exhibit stable recirculation zones.[4] Thus the tests reported here were designed with $Re_{D_b} > 2 \times 10^4$.

#### Cold-Flow Tests in Air

In general, the arguments for using water to simulate flow in combustion chambers apply as well to cold air except that visualization is much easier in water. The purpose of using cold airflow in this study was to provide easier measurements of mean velocity and turbulent intensity with a hot wire anemometer. The same model was used for both tests.

#### Residence Time Measurements

Residence time has been inferred from the decay of an injected tracer such as a salt solution.[7] After achieving steady state, the tracer is shut off, and the decay rate of concentration at a downstream station is monitored. If the flow through the device were "slug flow" at the average velocity, one would see nothing until $t = L_c A_b / \dot{w}$, when the signal would drop to zero. If there is recirculation over part of the cross section, the flow in other parts of the cross section will be at a higher speed than the average, so decay will start earlier. If there is substantial recirculation, some of the tracer will continue to "leak out" over longer times. The decay is usually plotted as

$$\xi(\bar{t}) = \ell n \left[ \frac{C(\bar{t})}{C(0)} \right] \tag{4}$$

where $\bar{t} \equiv t/(L_c A_b/\dot{w})$ and $C(\bar{t})$ and $C(0)$ are concentrations at $\bar{t}$ and just before shutoff.

We used warm water as the "tracer," since temperature is easier to monitor than salt concentration. Thus our equivalent of Eq. (4) is

$$\xi(\bar{t}) = \ell n \left[ \frac{T(\bar{t}) - T_s}{T_0 - T_s} \right] \tag{5}$$

## Apparatus and Instrumentation

#### Water Flow Visualization Facility

A schematic of the water facility is in Fig. 2. Two optical grade Plexiglas boxes are stacked vertically. The bottom contains the burner, and the top contains the afterburner. Refractive distortions are minimized with flat sides, since the boxes are always filled with water.

A flow rate of primary water of 0.23 m$^3$/min was chosen as nominal. This yields a Reynolds number of 27,800 and a bulk velocity of 0.165 m/s for a representative 17.1 cm i.d. burner can.

The flow was side-lighted and photographed using Polaroid ASA 3000 film at a shutter speed of 1/400 s at f/22 which showed the beads as short streaks. It was found that video tape recordings rendered the best visualization.

Beads injected into the flow upstream of the swirler were uniformly distributed by the central hub around the circumference of the swirler section. The purpose was to view large-scale flow features. Injection through the sidewall visualized specific points in the flow along the length and radius of the combustor. First, the PRZ could be investigated. Second, as the probes were moved incrementally toward the burner axis, the boundaries of the CRZ could be determined.

#### Air Cold-Flow Facility

The air cold-flow facility uses the same Plexiglas boxes and model. To provide primary air, an inlet pipe, a square-edge orifice plate, a blower, a diffuser, and a flow straightener were linked in sequence to the first box. A second blower with its own inlet and orifice provides secondary air.

With one purpose of the air facility being to compare air to water simulation, it was decided to match the Reynolds number of the air and water facilities. Thus, with the Reynolds number of the primary chamber fixed at 27,800, the bulk velocity of air became 3.2 m/s.

#### Burner Models

The basic model consists of a burner can with a swirl vane assembly (see Fig. 3). The burner can exhausts into an afterburner section where the primary flow is mixed with bypass air (see Fig. 4). The swirl vane assembly has 24 blades around the central hub. The blades are flat with chords varying from 1.60 cm at the root to 3.25 cm at the tip, with a span of 4.37 cm. The leading and trailing edges are rounded. This hub is unusually large for swirlers, 22.5% of burner area. However, in defining the confinement ratio the hub is not usually taken into account, giving for this burner $A_b/A_s = 1.0$. The lowest ratio the authors are aware of being previously investigated is $A_b/A_s = 2$ by Rhode and Lilley.[8]

The second configuration has the same swirl section but a larger-diameter (20.3-cm) burner can. The confinement ratio is increased to 1.4.

From these basic designs, several modifications were studied. These can be grouped into four categories: vane angle variations, different insert rings downstream of the swirler, central hub extensions, and changes in the diameter of the hub. The configurations are summarized and presented in Fig. 5. A geometric configuration will be referred to in the form "70-A," where "70" refers to vane angle, and "A" refers to the configuration in Fig. 5.

## Results

#### Water Flow Tests

The baseline design (see configuration A, Fig. 5) had a swirl vane setting of 70 deg to the combustor. It was found that no recirculation was evident. The vane angle was then increased to 80 deg. At this setting, a central zone of incipient recirculation was observed (see Fig. 6). Incipient recirculation is characterized by low axial velocities, high turbulence, and intermittent reverse flow over short distances. This is an unusually high vane angle for a swirl combustor, yet it was necessary to obtain any recirculation. As can be seen in the photograph, a slowly rotating toroidal zone is formed around the central reverse flow zone. This toroidal zone is thickest in the midsection of the burner can and then gradually decreases in cross-sectional area toward the end of the burner. There was also little swirling motion present in the reverse flow region, as has been reported for hubbed swirl combustors.[9]

In an attempt to strengthen recirculation, an outer ring was placed in the burner can immediately downstream of the swirl vanes (see Fig. 5, configuration B). The purpose of this was to increase the effective expansion ratio by first constricting the flow and then expanding it over the step. This modification strengthened the reverse flow region.

For the case of the larger burner can (see configuration E, Fig. 5), a vane angle of 80 deg produced mostly swirling flow through the combustor with only negligible recirculation. In this case, the addition of an insert ring was essential to produce some reverse flow (configuration F). The ring employed was of the same dimensions as used previously, with the exception that the outer diameter was extended to meet the inside diameter of the can. The resulting recirculation was of less strength than in the previous model (see Fig. 7). The slowly rotating toroidal zone was reduced in size, and the reverse flow was less intense.

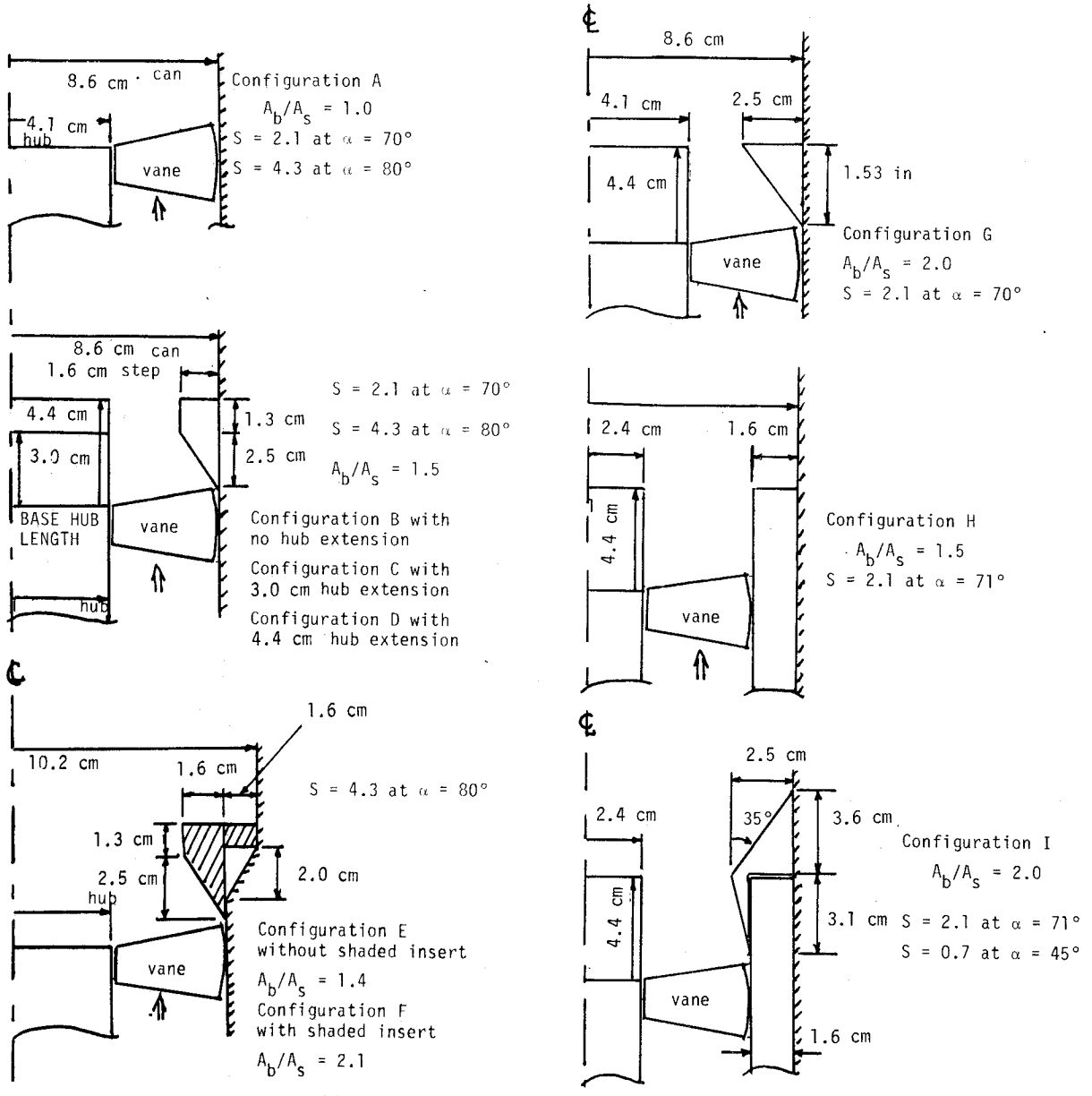


**Fig. 5 Diagrams of the various configurations tested.**

The present tracer decay results for both burner cans are shown in Fig. 8 along with some results from Ref. 3. A behavior such as shown is usually interpreted as indicating a "well-stirred reactor" followed by "plug flow" in the combustor. The residence time expressed as a fraction of the average burner can transit time is seen to decrease at the smaller confinement ratio. Of course, all of the swirl number values tested are high compared to the usually quoted critical value of $S \approx 0.6$ for unconfined (or slightly confined) flows. These results confirm the visualization tests.

Further modifications were tried to strengthen the recirculation at the 70-deg vane angle. First, extensions were placed on the central hub to bring the face of the hub in line with the end of the converging part of the ring and then with the step (configurations C and D). Features revealed by these tests can be summarized: 1) Along three-quarters of the burner axis there is a central zone of incipient recirculation of diameter approximately equal to the hub. 2) On the axis near the exit of the burner, an eddy forms at irregular intervals. When the eddy forms there is downstream flow in the central zone. On breaking up, reverse flow occurs. 3) There is no PRZ. 4) The swirling flow sticks on the hub face. These features are illustrated in Fig. 9.

The flowfield in the afterburner, without bypass flow, is shown in Fig. 9. A strand winds around the axis surrounded by a slowly swirling flow. The strand collapses in the upstream direction at irregular intervals. Whether this is associated with the burner can exit eddy is not clear.

Bypass flow changes the flow markedly. Figures 10a and 10b illustrate the flow in the primary can: 1) A core of small diameter forms along the axis of the burner. The core has low axial but high swirl velocity. It oscillates radially with high frequency and low amplitude, producing the snake-line appearance of Fig. 10b. 2) At irregular intervals the central zone collapses as in Fig. 10a. This produces a short period of relatively high recirculation compared to intermittent recirculation. 3) No PRZ forms. 4) Swirling flow sticks to the hub; however, to a lesser degree than in the no bypass case.

Bypass flow alters the flow in the afterburner, as shown in Figs. 11a and 11b. The single strand core from the burner can separates in two to form a rotating helix on entering the afterburner section. Above the helix is a region of high turbulence formed by eddies from the breaking strands. There is also an annulus of high-velocity flow around the helix. A schematic is shown in Fig. 12.

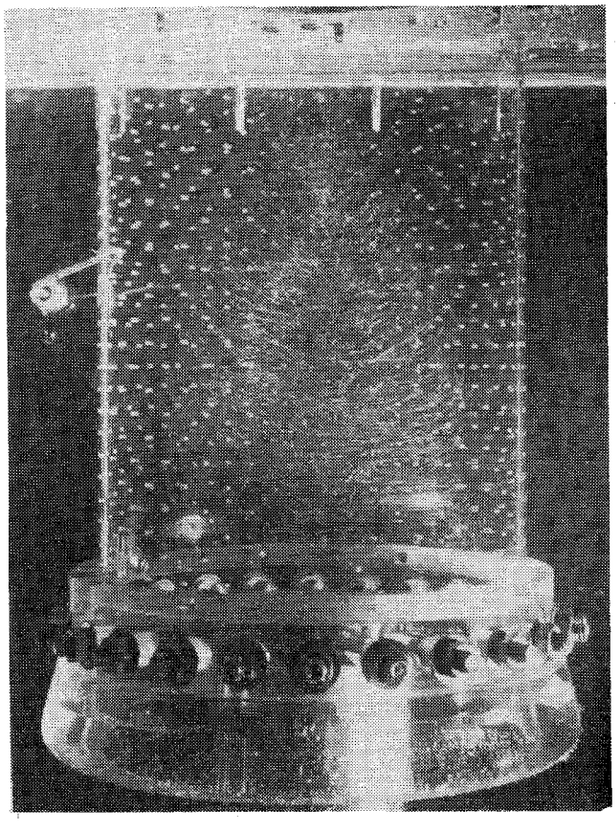

**Fig. 6 Flow pattern in 15.2-cm burner can: configuration 80-A with bypass flow.**

### Cold Airflow Tests

To make radial surveys of mean total velocity and turbulence intensity in the combustor, axial stations were chosen at the baseline hub face and $X/L_c = 0.10$, 0.15, 0.36, 0.49, 0.66, and 0.83 at downstream labeled stations No. 8, 7, 6, 5, 4, 3, and 2, respectively.

Both the mean and fluctuating velocities sensed with a straight hot wire aligned radially correspond to a velocity vector including only the axial and swirl components. The radial velocity component is assumed small.

The results for the long hub extension ("D") without and with bypass are shown in Figs. 13 and 14. Distinct changes occur with bypass flow. The velocity peaks tend to be increased and shifted toward the axis. Peak velocities at stations 2 and 3 are shifted from $r/D_b = 0.43$ without bypass to $r/D_b = 0.20$ with bypass, while at stations 4, 5, and 6, the peaks are shifted from $r/D_b = 0.43$ to $r/D_b = 0.35$. In the range $0.35 < r/D_b < 0.05$, velocities are generally higher at all stations with bypass flow. Also, velocities on the wall are slightly lower with bypass flow. Along most of the axis, normalized velocities are reduced by up to 20% with bypass flow. Without bypass flow and in the region $0.28 < r/D_b < 0.0$, the axial station with the highest velocity is station 4 followed by stations 3 and 2. Bypass flow reverses this order. On the axis, turbulence levels are greater by as much as 20% with bypass flow. From $0.50 < r/D_b < 0.13$, turbulence levels are much greater without bypass flow.

A test was conducted to determine the effect of closing the aspiration holes. Plastic wrap was wrapped around the burner can, leaving roughness due to the holes on the inside. The results with case "D" and bypass flow are shown in Fig. 15. It was found that velocities immediately along the wall increased approximately 25% and turbulence levels dropped by as much as 15% from $0.50 < r/D_b < 0.35$. In fact, except for station 6, the velocities at all stations were constant from the wall to $r/D_b = 0.28$. On the axis, turbulence and velocity were hardly

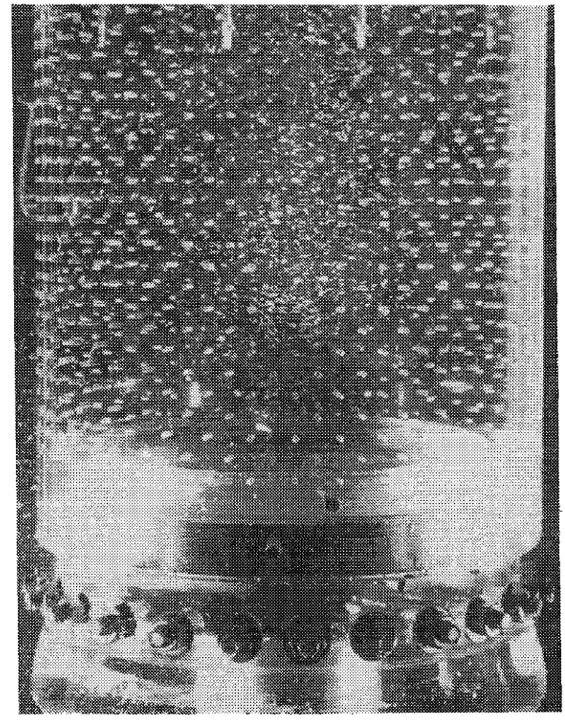

**Fig. 7 Flow pattern in 20.3-cm burner can: configuration 80-F.**

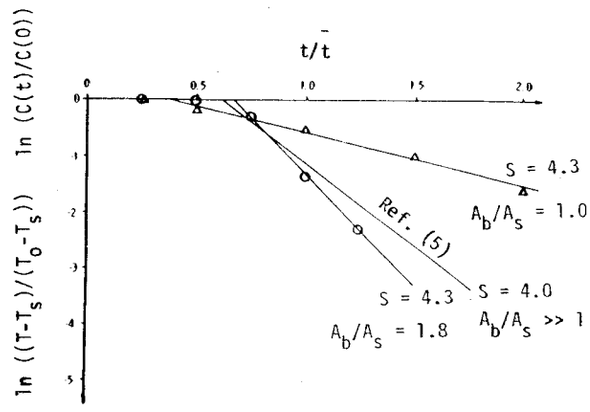


**Fig. 8 Dimensionless tracer decay rate for various confinement ratios.**

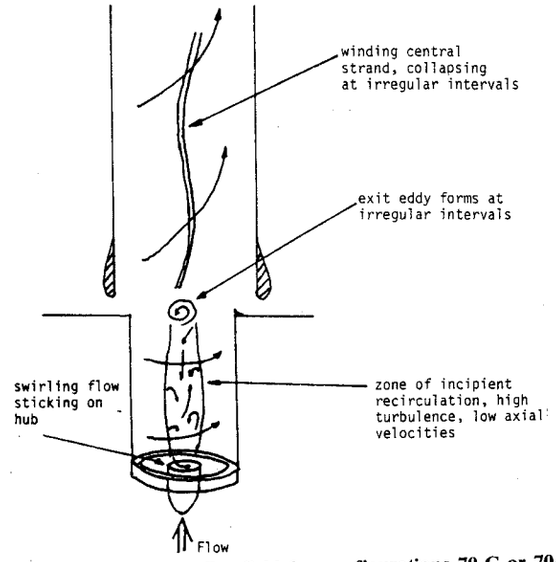


**Fig. 9 Schematic of the flowfield for configurations 70-C or 70-D without bypass flow.**

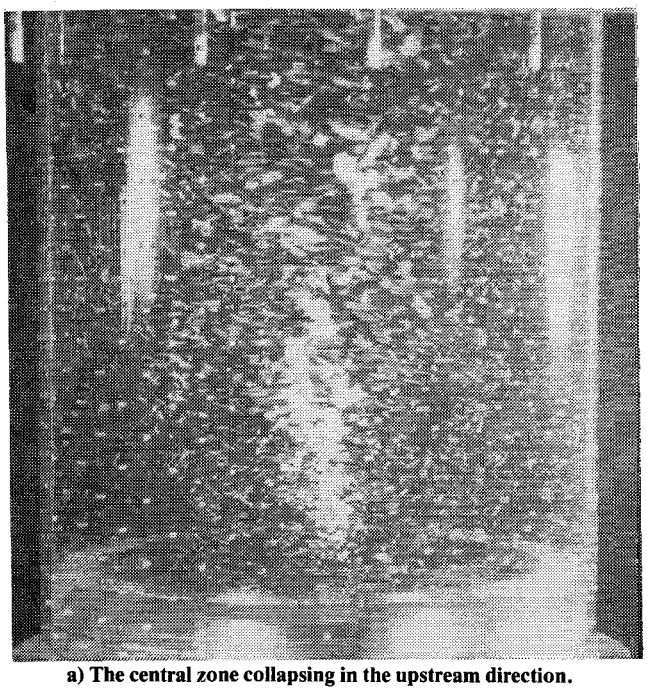

a) The central zone collapsing in the upstream direction.

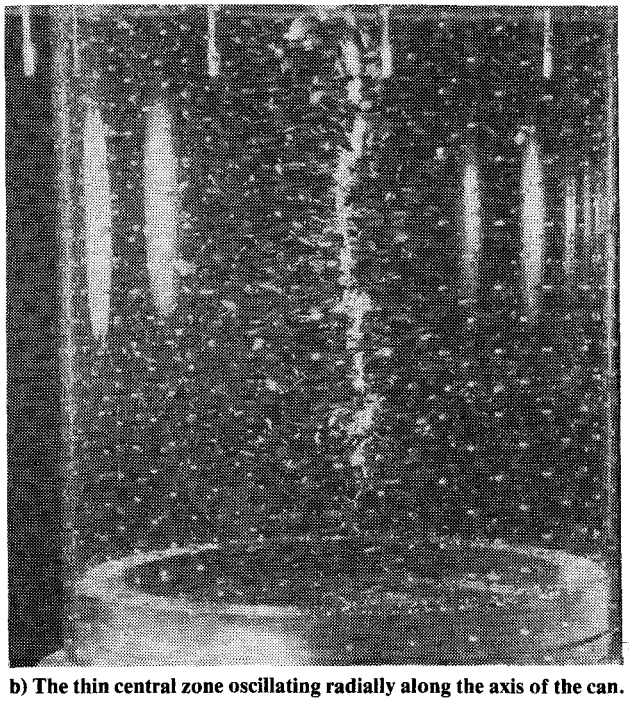

b) The thin central zone oscillating radially along the axis of the can.

Fig. 10 Flow patterns in the 15.2-cm burner can: configuration 70-C with bypass flow.

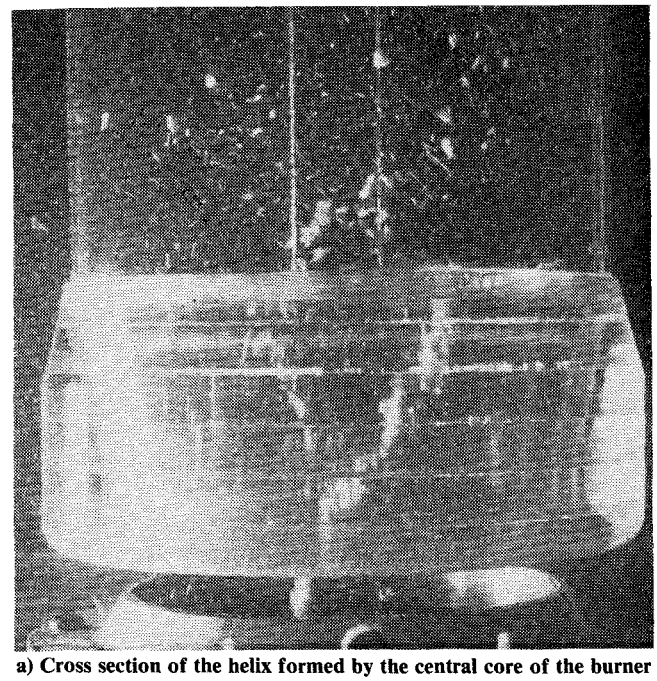

a) Cross section of the helix formed by the central core of the burner can breaking into two strands.

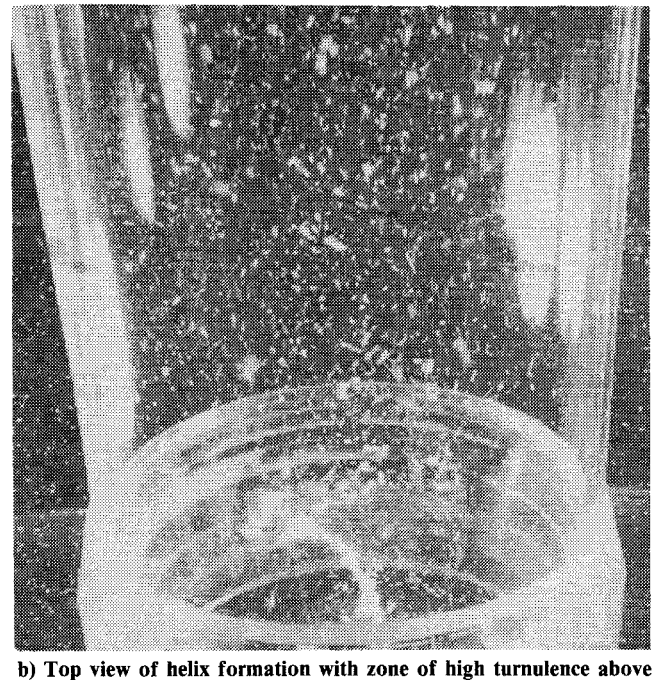

b) Top view of helix formation with zone of high turnulence above helix surrounded by annulus of bypass flow.

Fig. 11 Flow patterns in the afterburner: configurations 70-C and 70-D with bypass flow.

affected. The velocities at $r/D_b = 0.13$ and 0.05 are definitely lower without aspiration. The results of sealing the aspiraton holes are significant. Their purpose is to cool the liner; however, with the holes sealed, the velocity of the cold peripheral air is increased markedly, perhaps compensating for the loss of film cooling. Another beneficial effect of sealing the holes was to eliminate the low-velocity wake behind the step at $r/D_b = 0.50$ and 0.43 which might alleviate thermal problems.

The remaining parameter was hub diameter. A new configuration was developed with a smaller (but still "large") hub retaining the same swirl vanes and burner can shown in Fig. 5 (configuration H). The swirl and Reynolds number and Confinement Ratio were all the same as for the baseline design, requiring a vane angle increase to 71 deg. Data for this case are shown in Fig. 16 with bypass flow. Generally the smaller hub (71-H) produces a flatter profile with velocities lower by about 15% but the same turbulence profile as case 70-deg D, which had the larger hub. However, the radial stations for peak velocity at every axial station are the same in both the 71-H and 70-D cases. Stations 2 and 3 show the same linear, peaked profile for $0.50 \geq r/D_b \geq 0.2$ in both cases, and station 6 shows the same stepped velocity decay. These facts indicate that the basic flow mechanisms have not been changed. However, the station 4 profile is flat for $0.50 \geq r/D_b \geq 0.2$ for 71-H compared to a very curved profile for 70-D. Also, on the centerline, 71-H produces a drop in normalized velocity by about 20%, accompanied by a slight drop in turbulence level.

A convergent-divergent nozzle was added to the 71-H case to produce the 71-I configuration. The new design increased the confinement ratio to 2.0. The results with bypass flow are

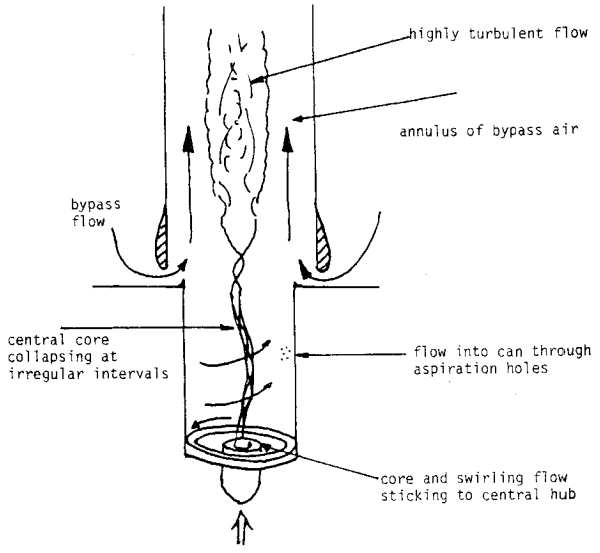


**Fig. 12 Schematic of the flowfield in configuration 70-C or 70-D with bypass flow.**

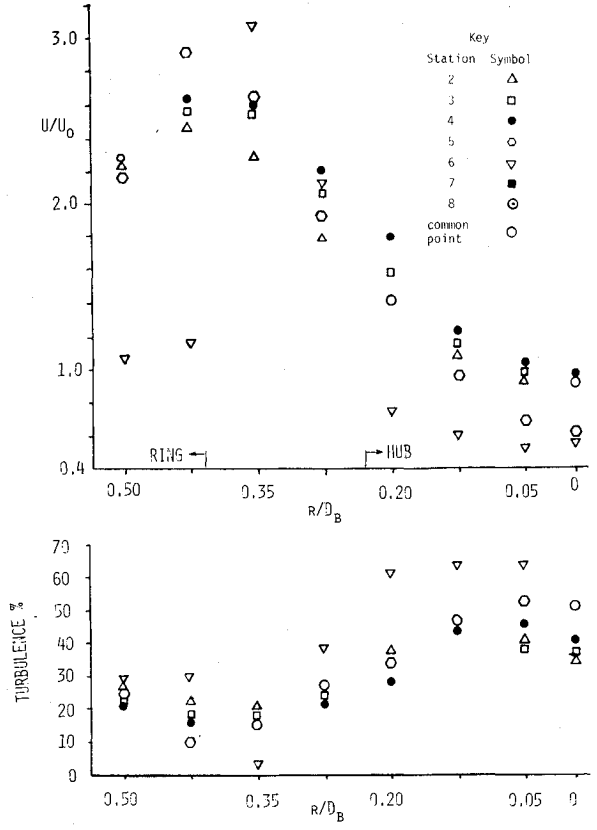


**Fig. 13 Hot wire velocity and turbulence level measurements for configuration 70-D without bypass flow.**

shown in Fig. 17. No major differences were found when compared to 71-H, except on the axis, where there is a further, uniform decrease in velocity of 20% and an increase in turbulence level of 10%—both beneficial effects.

The very high vane angles used up to this stage were unusual for most swirl combustors. Therefore a series of tests was run at 45 deg, producing a swirl number one-third of that earlier. Comparing 45-I (Fig. 18) to 71-I (Fig. 17) does show the effect of degree of swirl. Profiles at stations 2 and 3 become smooth from $0.50 \leq r/D_b \leq 0.13$ with 45-I, while they are straight at the higher angle. Lower average velocities from

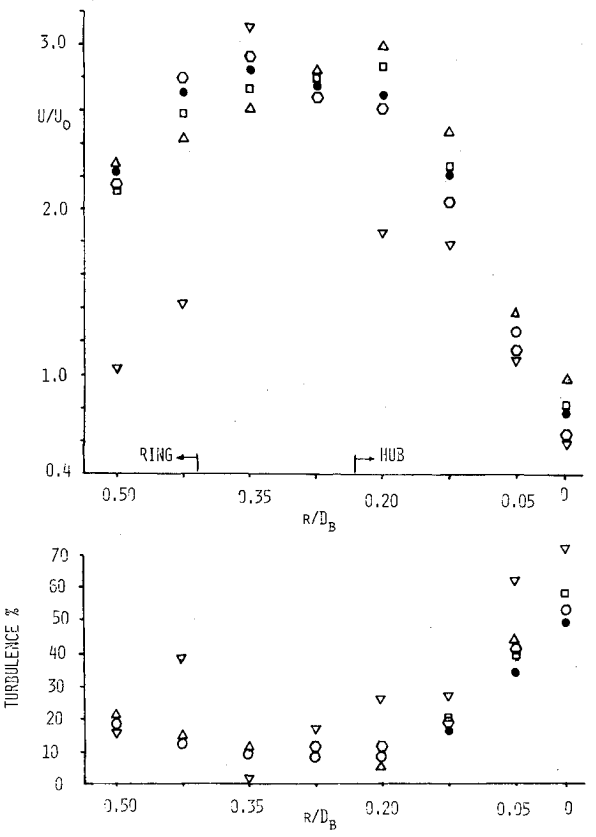


**Fig. 14 Hot wire velocity and turbulence level measurements for configuration 70-D with bypass flow.**

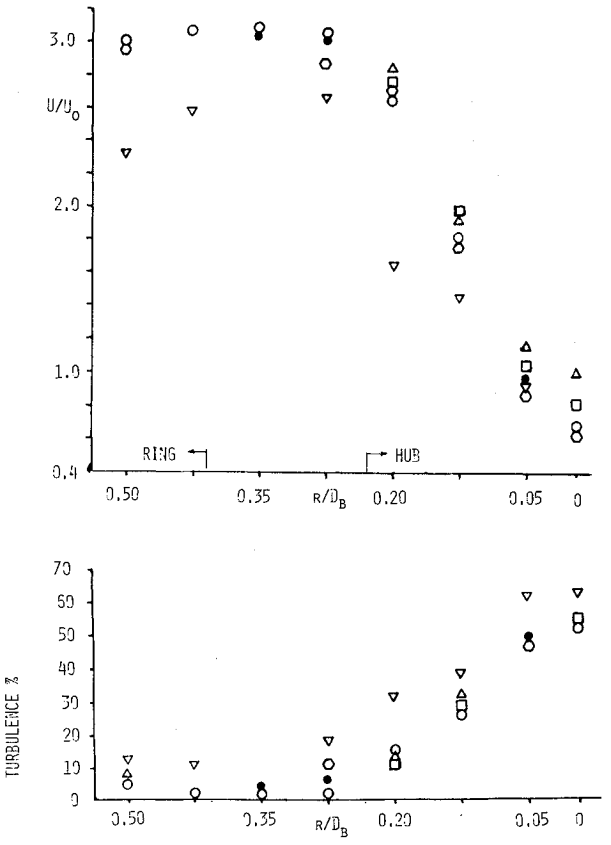


**Fig. 15 Hot wire velocity and turbulence level measurements for configuration 70-D, without aspiration, with bypass flow.**

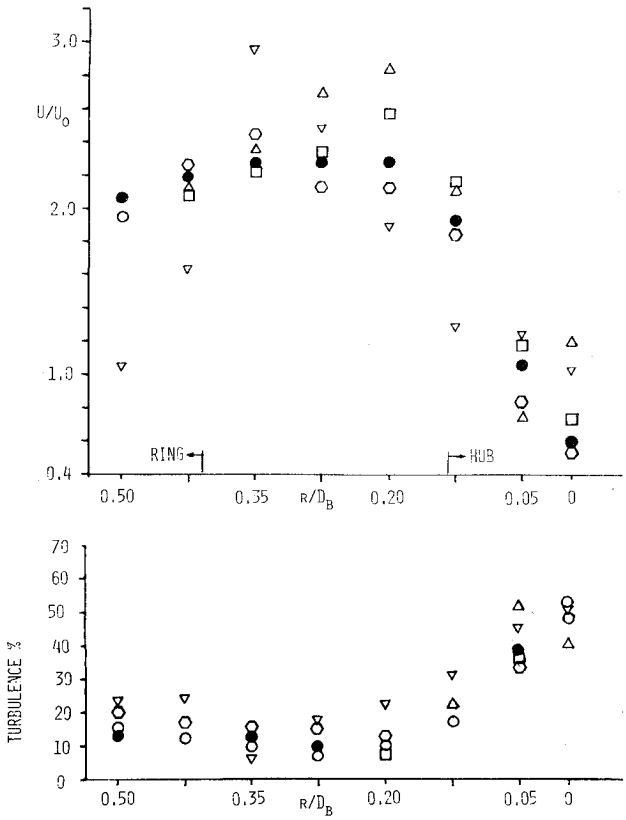


Fig. 16 Hot wire velocity and turbulence level measurements for configuration 71-H with bypass flow.

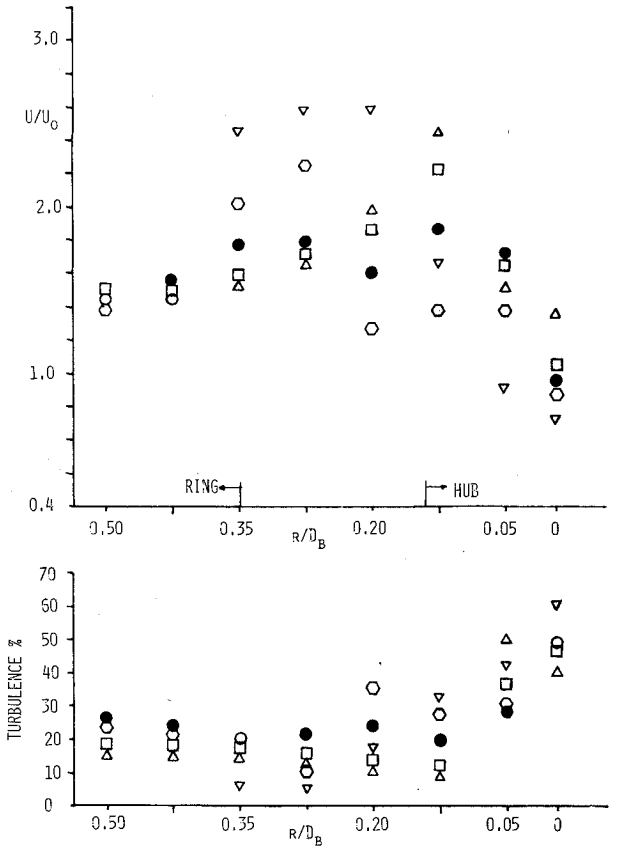


Fig. 18 Hot wire velocity and turbulence level measurements for configuration 45-I with bypass flow.

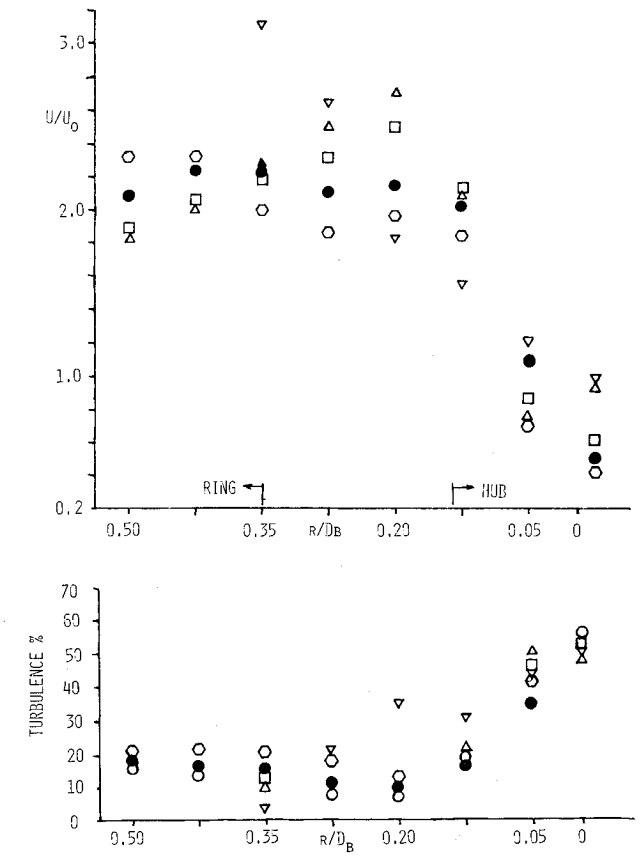


Fig. 17 Hot wire velocity and turbulence level measurements for configuration 71-I with bypass flow.

$0.50 \leq r/D_b \leq 0.20$ and turbulence levels, but a sharp increase in centerline velocity are also the effects of a lower angle.

## Conclusions

The design features which are likely to affect the flow characteristics of the combustor under consideration were tested: swirl vane angle, confinement ratio, secondary injection rate, aspiration, and the length and diameter of the central hub. Also, a converging-diverging burner entrance was tested.

Most of the tests were done with a high vane angle (70 deg) because of the low confinement ratio of the combustor. An increase to 80 deg produced a greater tendency to recirculate. A decrease to 45 deg lessened the tendency to recirculate.

Increasing the confinement ratio directly by increasing the diameter of the burner can did not strengthen the incipient recirculation. Increasing the effective confinement ratio by inserting a ring after the swirler was necessary to produce incipient recirculation at 70 deg. Further increases in the effective confinement ratio produced still lower axial velocities on the axis.

The effect of increasing bypass flow ratio from 0 to 2 generally increased total velocities and shifted peak velocities at most axial stations closer to the axis in the burner, but left velocities on the axis unchanged. Turbulence was also concentrated near the axis in a thin region of incipient recirculation.

The effect of sealing aspiration holes was to increase velocities and decrease turbulence near the burner wall. Velocity decay was enhanced near the axis. The low-velocity wake behind the step was eliminated.

Extending the large-diameter hub by 0.38 and 0.54 diameters produced only small effects on the flow in the burner. Larger effects were noted in the afterburner. Upon entering the afterburner for a swirler with an extended hub, the central core split into a rotating helix when bypass flow

was added. Without bypass flow, a central core of diameter equal to the hub in the burner, an eddy at the burner exit, and a winding core in the afterburner were created.

Decreasing the area of the extended hub while maintaining fixed values of the swirl number, the Reynolds number, and the confinement ratio resulted in lower axial velocities along most of the centerline but still no steady reversed flow.

The insertion of a converging-diverging ring in the burner after the swirler with the small hub produced a further drop in the axial velocity and an increase in turbulence over the length of the burner.

By virtue of requirements for wall cooling, and vehicle constraints, the baseline combustor exhibits a design that is, in a sense, new on the basis of previous swirl burner practices. No steady actual upstream flow was found in the burner, although variations of most all the major parameters were tested. However, large zones of lower axial velocities with high turbulence were found in some cases. This may be adequate for effective flame holding and efficient combustion.

## Acknowledgments

These studies were supported by the Atlantic Research Corporation. Technical monitoring was by William Sargent and Frederick Rodgers.

## References

[1]Buckley, P. L., Craig, R. R., Davis, D. L., and Schwartzkoff, K. G., "The Design and Combustion Performance of Practical Swirlers for Integral Rocket/Ramjets," AIAA Paper 80-1119, 1980.

[2]Syred, N. and Dahman, K. R., "Effect of High Levels of Confinement Upon the Aerodynamics of Swirl Burners," *Journal of Energy*, Jan.-Feb. 1978, pp. 8-15.

[3]Beer, J. M. and Lee, K. B., "The Effect of Residence Time Distribution on the Performance and Efficiency of Combustors," *10th Symposium (International) on Combustion*, 1965, pp. 1187-1202.

[4]Syred, N. and Beer, J.M., "Combustion in Swirling Flows: A Review," *Combustion and Flame*, 1974, pp. 143-201.

[5]Combustion and Systems—Water Analogy Facility, Rolls-Royce Limited Aero Division, Bristol, England.

[6]Syred, N., Chigier, N. A., and Beer, J. M., "Flame Stabilization in Recirculation Zones of Jets with Swirl," *13th Symposium (International) on Combustion*, The Combustion Institute, Pittsburgh, Pa., 1971, pp. 617-624.

[7]Beer, J. M. and Chigier, N. A., *Combustion Aerodynamics*, Halsted-Wiley, New York, 1972.

[8]Rhode, D. L. and Lilley, D. G., "Mean Flowfields in Axisymmetric Combustor Geometries with Swirl," AIAA Paper 82-0177, 1982.

[9]Beer, J. M., "On the Stability and Combustion Intensity of Pressure-Jet Oil Flames," *Combustion*, Vol. 37, 1965, pp. 27-49.